Resonant Raman scattering by longitudinal-optical phonons in $Zn_{1-x}Mn_xSe$ ($x=0$, 0.03, 0.1) near the E_0 gap

W. Limmer, H. Leiderer, K. Jakob, and W. Gebhardt
Institut für Festkörperphysik, Universität Regensburg, Universitätsstrasse 31, D-8400 Regensburg, Federal Republic of Germany

W. Kauschke,* A. Cantarero,† and C. Trallero-Giner‡
Max-Planck-Institut für Festkörperforschung, Heisenbergstrasse 1, Postfach 80 06 65, D-7000 Stuttgart 80, Federal Republic of Germany

(Received 7 May 1990)

The efficiency of resonant one- and two-LO-phonon Raman scattering in oriented cubic $Zn_{1-x}Mn_xSe$ single crystals with $x=0, 0.03, 0.1$ is studied for incident photon energies near the E_0 fundamental band gap. Absolute values of the Raman scattering efficiency (RSE) are determined for several backscattering configurations by using a sample substitution method and by correcting the measured intensities with respect to absorption, reflection, and refraction. The experimental data for one-LO-phonon scattering via deformation-potential and Fröhlich electron-phonon interaction are quantitatively compared with model calculations for the absolute RSE, where bound and continuum exciton states are considered as intermediate electronic states. Near resonance, strong LO-phonon intensities are measured in backscattering configurations where scattering via the deformation-potential and Fröhlich interaction is forbidden according to the standard Raman selection rules.

I. INTRODUCTION

Raman scattering by one (two) LO phonon(s) is usually described in time-dependent perturbation theory as a three- (four-) step process where a part of the photon energy is transferred to the phonon system via intermediate electronic states.[1,2] A resonant enhancement of the Raman scattering efficiency (RSE) occurs whenever the energy of the incident or scattered photon approaches a critical point in the combined density of electronic band states. A quantitative comparison of the resonance behavior and the absolute values of the RSE with theoretical calculations yields detailed information about the electron-phonon interactions and the intermediate electronic states involved in the scattering process. Furthermore, band-structure parameters such as gap energy E_0, excitonic broadening Γ, and the optical deformation potential $D_{\rm opt}$ can be obtained. In polar semiconductors there are two different mechanisms of electron-phonon interaction. The first one is caused by the deformation potential and the second one, the Fröhlich interaction, is due to the macroscopic electric field accompanying the LO phonons. The deformation-potential electron-phonon interaction and an electro-optic mechanism, which arises from the interband matrix elements of the Fröhlich electron-phonon interaction, lead to the usual selection rules of dipole-allowed LO-phonon scattering. The electro-optic contribution is expected to be small compared to the deformation-potential interaction and is neglected, or implicitly included in a slightly renormalized electron-phonon interaction, when calculating the RSE for dipole-allowed resonant Raman scattering (RRS). Dipole-forbidden LO-phonon scattering is due to the **Q**-dependent intraband matrix elements of the Fröhlich interaction, where **Q** denotes the scattering wave vector. Choosing appropriate backscattering configurations, dipole-allowed and dipole-forbidden scattering can be observed separately. In the last few years several publications have been devoted to the RRS in III-V semiconductors,[3-9] semiconductor alloys,[10,11] and superlattices.[12] Taking into account uncorrelated electron-hole pairs as intermediate electronic states, the observed resonance spectra for the intraband Fröhlich interaction at critical points higher than the fundamental gap E_0 have been explained by assuming an impurity-induced scattering mechanism.[13] This means that the electron-hole pair is scattered twice, once inelastically by the electron-phonon interaction and once elastically by an electron-impurity process. Near the E_0 gap an impurity-induced scattering mechanism also qualitatively describes the resonance behavior of the RSE for both the deformation potential and Fröhlich interaction.[14] However, the calculated absolute values are about 1 to 2 orders of magnitude smaller than the experimental values. Recently it has been shown that in the case of III-V semiconductors good agreement between experiment and theory can be achieved if the discrete and continuous states of Wannier-Mott excitons are considered as intermediate electronic states for scattering near the E_0 and $E_0+\Delta_0$ band gaps.[15,16] No additional elastic scattering by impurities had to be taken into account to describe

quantitatively the experimental results in undoped samples.

In this paper we report on resonant Raman scattering by one and two LO phonons near the E_0 gap in the II-VI semiconductors $Zn_{1-x}Mn_xSe$ with $x=0$, 0.03, and 0.1.

II. THEORY

For a quantitative comparison of experimental and theoretical results it is convenient to use the Raman scattering efficiency $dS/d\Omega$ as a measure of the scattered Raman intensities.[1,2] This quantity has the dimension of an inverse length and represents the ratio between scattered and incident power for a unit solid angle and a unit path length within the crystal. It is defined as

$$\frac{dS}{d\Omega} \equiv \frac{dP_S}{d\Omega}\frac{1}{P_L L} , \tag{1}$$

where $dP_S/d\Omega$ denotes the scattered power per solid angle $d\Omega$ inside the crystal, P_L is the incident power, and L is the scattering length. In a microscopic description of the scattering process the RSE is related to the scattering amplitude W_{fi} which describes the transition from the initial state i to a final state f:[17]

$$\frac{dS}{d\Omega} = \frac{\omega_S}{\omega_L}\frac{n_L}{c}\frac{1}{d\Omega}\frac{2\pi}{\hbar}\sum_f |W_{fi}|^2 \delta(E_i - E_f) , \tag{2}$$

where ω is the photon frequency, n is the index of refraction, and c is the speed of light in vacuum. The quantities referring to the incident and scattered photons have subscripts L and S, respectively. E_i and E_f are the energies of the initial and final state, respectively. For intrinsic Stokes scattering by one LO phonon the scattering amplitude can be evaluated in third-order perturbation theory, leading to a sum of six different terms. The most resonant one is given by[2,18]

$$W_{fi}(1\ \mathrm{LO};\mathrm{int}) = \sqrt{\bar{n}+1}\sum_{\alpha,\beta}\frac{\langle 0|H_{eR}^{+}(\hat{\mathbf{e}}_S)|\beta\rangle\langle\beta|H_{eL}|\alpha\rangle\langle\alpha|H_{eR}^{-}(\hat{\mathbf{e}}_L)|0\rangle}{(E_\beta - \hbar\omega_S)(E_\alpha - \hbar\omega_L)} , \tag{3}$$

where $\bar{n}$ is the phonon occupation number and $|0\rangle$ the electronic ground state, with all valence bands occupied and all conduction bands empty, $H_{eR}^{-}(\hat{\mathbf{e}}_L)$ and $H_{eR}^{+}(\hat{\mathbf{e}}_S)$ are the electron-photon interaction operators for the absorption and emission of the incident and scattered photon, respectively, $\hat{\mathbf{e}}_L$ and $\hat{\mathbf{e}}_S$ are the corresponding polarization vectors, and H_{eL} is the electron-phonon interaction operator. The summation in Eq. (3) has to be carried out over all intermediate electronic states α and β. The RSE can also be expressed by the corresponding Raman tensor $\overleftrightarrow{R}$ (Refs. 4 and 14) as

$$\frac{dS}{d\Omega} = \frac{\omega_S^3\omega_L}{c^4}\frac{\hbar^2}{2v_c M^* \hbar\Omega_{\mathrm{LO}}}\frac{n_S}{n_L}(\bar{n}+1)|\hat{\mathbf{e}}_S^{*}\cdot\overleftrightarrow{R}\cdot\hat{\mathbf{e}}_L|^2 , \tag{4}$$

where Ω_{LO} is the LO-phonon frequency, v_c is the volume of the primitive cell, and M^* its reduced mass. In the case of scattering by two LO phonons the expressions for the scattering amplitude and the RSE are very similar to those of Eqs. (3) and (4) and can be found in Refs. 19 and 20.

For backscattering at the $(00\bar{1})$ and $(0\bar{1}\,\bar{1})$ surfaces of zinc-blende-type crystals the Raman tensors for one-LO-phonon scattering via the deformation-potential (DP) interaction and via the intraband Fröhlich (F) interaction are given by[1,2]

$$\overleftrightarrow{R}_{\mathrm{DP}}(00\bar{1}) = \begin{pmatrix} 0 & a_{\mathrm{DP}} & 0 \\ a_{\mathrm{DP}} & 0 & 0 \\ 0 & 0 & 0 \end{pmatrix} ,$$

$$\overleftrightarrow{R}_{\mathrm{DP}}(0\bar{1}\,\bar{1}) = \frac{1}{\sqrt{2}}\begin{pmatrix} 0 & a_{\mathrm{DP}} & a_{\mathrm{DP}} \\ a_{\mathrm{DP}} & 0 & 0 \\ a_{\mathrm{DP}} & 0 & 0 \end{pmatrix} , \tag{5}$$

$$\overleftrightarrow{R}_F(00\bar{1}) = \overleftrightarrow{R}_F(0\bar{1}\,\bar{1}) = \begin{pmatrix} a_F & 0 & 0 \\ 0 & a_F & 0 \\ 0 & 0 & a_F \end{pmatrix} .$$

Analytical expressions for the complex Raman polarizabilities a_{DP} and a_F near the critical points E_0 and $E_0+\Delta_0$ can be found in Refs. 15 and 16. Using the Wannier-Mott exciton model in effective-mass approximation, the discrete and continuous states of heavy, light, and split-off excitons have been taken into account as intermediate electronic states of the scattering process. The resonance behavior of the Raman polarizabilities a_{DP} and a_F, obtained by using different Bohr radii for the excitons, does not differ significantly from that with one effective Bohr radius $\bar{a}$. Thus, in the following the theoretical results will be applied to the simple case in which the same effective Bohr radius $\bar{a}$, Rydberg energy E_{Ry}, and

broadenings Γ are assumed for all excitons. For the broadenings Γ_n of the discrete exciton states we use the empirical relation[15]

$$\Gamma_n=\Gamma_c-(\Gamma_c-\Gamma_1)/n^2,\quad n=1,2,3\ldots \tag{6}$$

where Γ_1 denotes the broadening of the $n=1$ discrete and Γ_c the broadening of the continuous excitonic states. In the case of scattering by one LO phonon via deformation-potential interaction the Raman polarizability $a_{\rm DP}$ can be written as[15]

$$a_{\rm DP}=K_{\rm DP}\sum_{p,q} D_{p,q}(\hbar\omega_L)+b_{\rm DP}\ , \tag{7}$$

where the sum in p,q runs over the heavy, light, and split-off excitons, $b_{\rm DP}$ is a background coming from nonresonant processes, and the factor $K_{\rm DP}$ is given by

$$K_{\rm DP}=\frac{a_0^2}{2\pi\sqrt{3}}\left[\frac{R_{\rm H}}{E_{\rm Ry}}\right]^2\left[\frac{a_{\rm H}}{\bar{a}}\right]^3\frac{P^2}{m_0}\frac{D_{\rm opt}}{\hbar\omega_L(\hbar\omega_L\hbar\omega_S)^{1/2}}\ . \tag{8}$$

Here, a_0 is the lattice constant, $R_{\rm H}$ and $a_{\rm H}$ are the Rydberg energy and the Bohr radius of the hydrogen atom, respectively, P is the real interband matrix element of the momentum operator,[1] m_0 the free-electron mass, and $D_{\rm opt}$ the optical deformation potential. $D_{\rm opt}$ is defined as

$$D_{\rm opt}\equiv\frac{2a_0}{\sqrt{3}}\langle X|V_{{\rm DP},z}|Y\rangle\ , \tag{9}$$

where X and Y are the p_x and p_y valence-band wave functions at the Γ point of the Brillouin zone[21] and $V_{{\rm DP},z}$ is the derivation of the electronic potential with respect to a relative sublattice displacement along the z direction. The resonant function $D_{p,q}(\hbar\omega_L)$ in Eq. (7) describes a process where the intermediate electronic state is scattered from exciton p to exciton q via the interband matrix elements of the deformation-potential interaction.

The Raman polarizability a_F for scattering via intraband Fröhlich interaction can be written as[16]

$$a_F=K_F\sum_p F_p(\hbar\omega_L)\ , \tag{10}$$

where the sum in p runs over the heavy, light, and split-off excitons and the factor K_F is given by

$$K_F=\frac{2}{\pi}\left[a_0^3\frac{M^*}{m_0}\frac{\hbar\Omega_{\rm LO}}{R_{\rm H}}\right]^{1/2}\frac{a_{\rm H}QC_F}{\hbar\omega_L(\hbar\omega_L\hbar\omega_S)^{1/2}}\times\frac{2}{3}\frac{P^2}{m_0}\frac{a_{\rm H}}{\bar{a}}\left[\frac{R_{\rm H}}{E_{\rm Ry}}\right]^2. \tag{11}$$

Q denotes the phonon wave number and C_F the Fröhlich constant which is defined as

$$C_F=e\left[2\pi\hbar\Omega_{\rm LO}\left[\frac{1}{\epsilon_\infty}-\frac{1}{\epsilon_0}\right]\right]^{1/2}, \tag{12}$$

where e is the free-electron charge, ϵ_0 the static dielectric constant, and ϵ_∞ the high-frequency dielectric constant. The function $F_p(\hbar\omega_L)$ represents the resonant contribution to the RSE which arises from the intraband scattering of exciton p.

III. EXPERIMENTAL DETAILS

Absolute values of the RSE were obtained by using a sample substitution method[1] with the 524 $\rm cm^{-1}$ LO-phonon line of high-purity Si as a reference.[22] The measured scattering rates R of sample and R^* of reference outside the crystal are related to the Raman efficiency by[1,2]

$$\frac{dS}{d\Omega}(\omega_L)=\frac{K^*(\omega_L,\omega_S)}{K(\omega_L,\omega_S)}\frac{dS^*}{d\Omega}(\omega_L)\frac{R(\omega_L)}{R^*(\omega_L)} \tag{13}$$

with

$$K(\omega_L,\omega_S)\equiv\frac{(1-r_L)(1-r_S)\{1-\exp[-(\alpha_L+\alpha_S)L]\}}{n_S^2(\alpha_L+\alpha_S)}\ . \tag{14}$$

The frequency-dependent factors $K(\omega_L,\omega_S)$ and $K^*(\omega_L,\omega_S)$ must be used to correct the measured scattering rates with respect to absorption (α), reflectivity (r), and refraction (n). The optical constants of the $Zn_{1-x}Mn_xSe$ samples were obtained from transmission and reflectivity measurements at our laboratory and completed by absorption data from Ref. 23. The corresponding data for Si were taken from Refs. 24 and 25. For the absolute RSE of Si we use the empirical relation

$$\left[\frac{dS^*}{d\Omega}\right]_{\rm Si}(\omega_L)=(7.75\times10^{-5})(\hbar\omega_L-3.4)^{-4}\ , \tag{15}$$

in $\rm sr^{-1}\,cm^{-1}$, with $\hbar\omega_L$ in eV, which represents a good interpolation of the experimental data given in Ref. 22. In Fig. 1 the normalized Raman intensity R/R^* and the corresponding RSE are shown for one-LO-phonon scattering in ZnSe using the $z(x,x)\bar{z}$ backscattering configuration. While the variation of r and n near the E_0

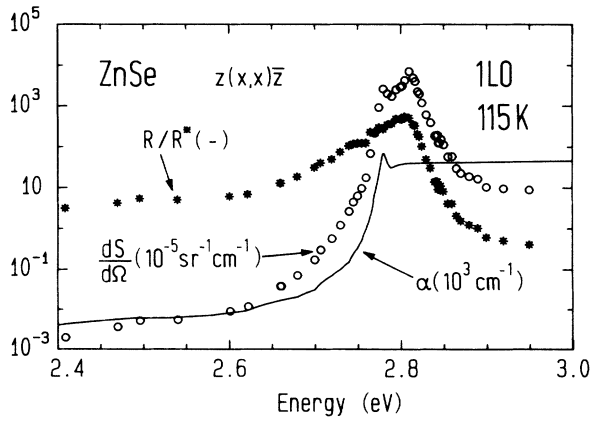

FIG. 1. The absolute Raman scattering efficiency $dS/d\Omega$ for $z(x,x)\bar{z}$ in ZnSe is obtained from the corresponding normalized Raman intensity R/R^* using Eqs. (13) and (14). The absorption coefficient α of ZnSe is shown for comparison.

gap is less than 15% for temperatures above 80 K, the absorption coefficient α increases by several orders of magnitude. Hence, the frequency dependence of the factor $K(\omega_L,\omega_S)$ is mainly determined by α.

For the Raman measurements a cw dye laser operating with stilbene 3 and pumped by the uv lines of an Ar^+-ion laser was used as a tunable excitation source in the spectral range 2.64–2.95 eV. In the range 2.40–2.65 eV the visible single lines of an Ar^+-ion laser were used. The laser beam was focused onto the sample with a cylindrical lens. Sample and reference were mounted on the cold finger of a temperature variable N_2 cryostat. The detection system was computer controlled and consisted of a Jarrel-Ash 1 m double-grating monochromator with a RCA 31034 GaAs photomultiplier tube connected to a photon-counting system. The measured intensities were stored in a computer system which enabled us to subtract the background in the Raman spectra by appropriate computer programs. All measurements were performed in backscattering configurations with the direction of incident and scattered light perpendicular to the $(00\bar{1})$ or $(0\bar{1}\,\bar{1})$ surface of the samples. We denote the [100], [010], [001], $[1\bar{1}0]$, [110], $[01\bar{1}]$, and [011] directions of the crystal by x, y, z, x', y', y'', and z'', respectively. The sample surfaces were oriented in the $[00\bar{1}]$ and $[0\bar{1}\,\bar{1}]$ directions using an optical two-circle reflection goniometer and the orientation was finally checked by the Laue method. The surfaces were polished on a microcloth saturated with a suspension of 0.05 μm alumina powder in distilled water. Table I shows the scattering configurations used in this work and the corresponding Raman polarizabilities for one-LO-phonon scattering $|\hat{e}_S^*\cdot\vec{R}\cdot\hat{e}_L|^2$ derived from Eq. (5). It should be noted that the [110] and $[1\bar{1}0]$ directions are physically inequivalent in II-VI compounds and that the labeling depends on the position of cations and anions in the coordinate system.[3] These positions can be determined by inspection of the etch patterns produced by preferential etching of the (001) surface. As will be shown later, we obtained the same experimental results for the $z(x',x')\bar{z}$ and $z(y',y')\bar{z}$ scattering configurations. Therefore, the etching procedure has been omitted. The measurements on $Zn_{0.97}Mn_{0.03}Se$ and $Zn_{0.9}Mn_{0.1}Se$ were carried out at 80 K. For ZnSe we used a temperature of 115 K in order to avoid a large photoluminescence background in the Raman spectra arising from free-to-bound transitions.[26,27] Figure 2 shows the photoluminescence spectra of ZnSe at the temperatures $T=95$, 115, and 150 K, using an excitation laser energy of 2.815 eV and a $z(x,x)\bar{z}$ backscattering configuration. For increasing temperature the free-to-bound transition luminescence with maximum at 460 nm decreases rapidly and the band-edge emission E is shifted to lower energies. The Raman lines for scattering by one, two, and three LO phonons are clearly discernible.

TABLE I. Scattering configurations and corresponding Raman polarizabilities, investigated in this paper.

Scattering configuration	$\lvert\hat{e}_S^*\cdot\vec{R}\cdot\hat{e}_L\rvert^2$
$z(y,x)\bar{z}$	$\lvert a_{DP}\rvert^2$
$z(x,x)\bar{z}, z''(x,x)\bar{z}''$	$\lvert a_F\rvert^2$
$z(x',x')\bar{z}$	$\lvert a_F-a_{DP}\rvert^2$
$z(y',y')\bar{z}$	$\lvert a_F+a_{DP}\rvert^2$
$z(y',x')\bar{z}, z(x',y')\bar{z}$	0
$z''(y'',x)\bar{z}''$	0

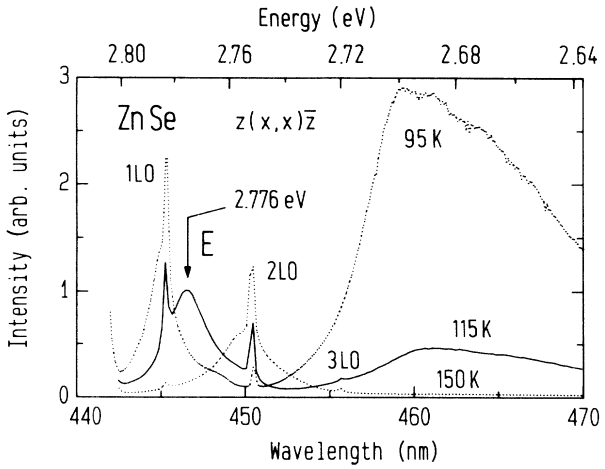

FIG. 2. Photoluminescence spectra of ZnSe at the temperatures 95, 115, and 150 K using an excitation laser energy of 2.815 eV.

IV. RESULTS AND DISCUSSION

A. Scattering by one LO phonon

In this section the experimental resonance behavior of the RSE for scattering by one LO phonon in $Zn_{1-x}Mn_xSe$ ($x=0,0.03,0.1$) will be presented for several backscattering configurations and compared with theory. Absolute values for the experimental RSE were determined from the measured Raman intensities by using the procedure described in Sec. III. Theoretical resonance curves were obtained from numerical calculations using Eq. (4) and the Raman polarizabilities a_{DP} and a_F from Refs. 15 and 16, respectively. All parameters used for the numerical calculations, with the exception of gap energy E_0, exciton Bohr radius $\tilde{a}$ and excitonic broadenings Γ, were taken from the literature. They are summarized in Table II. In order to obtain one effective Bohr radius $\tilde{a}$ for all excitons, we calculate the hypothetical Bohr radii a and Rydberg energies E_{Ry} of heavy and light excitons from the well-known relations

$$a=a_H\frac{m_0\epsilon}{\mu},\quad E_{Ry}=R_H\frac{\mu}{m_0\epsilon^2}\ , \tag{16}$$

where μ denotes the reduced effective mass of electron and hole and ϵ the dielectric constant. Using for m_e, m_h, and $\epsilon=\epsilon(0)$ the values from Table II, we obtain for the heavy exciton $a=38$ Å, $E_{Ry}=21$ meV and for the light exciton $a=66$ Å, $E_{Ry}=12$ meV. From a comparison with the experimental value $E_{Ry}=19$ meV (Ref. 28) we deduce an effective Bohr radius $\tilde{a}=42$ Å. The values of

TABLE II. Numerical values of the parameters used for the theoretical curves.

ZnSe	
$E_0=2.800$ eV	$\bar{a}=42$ Å [d]
$E_{Ry}=19$ meV [a]	$Q=8\times10^{-3}$ Å^{-1} [e]
$\Delta_0=0.403$ eV [a]	$m_e=0.15m_0$ [a]
$\hbar\Omega_{LO}=31.5$ meV [b]	$m_{lh}=0.14m_0$ [a]
$\Gamma_i=4$ meV	$m_{hh}=0.78m_0$ [a]
$\Gamma_c=16$ meV	$m_{s.o.}=0.28m_0$ [f]
$a_0=5.67$ Å [a]	$M^*=35.8$ amu
$D_{opt}=12$ eV [c]	$P^2/m_0=9.4$ eV [g]
$\epsilon(0)=9.0$ [a]	$\epsilon(\infty)=5.5$ [a]
$b_{DP}=0$ Å^2	
$Zn_{0.97}Mn_{0.03}Se$	
$E_0=2.789$ eV	$\Gamma_c=40$ meV
$\Gamma_i=10$ meV	
$Zn_{0.9}Mn_{0.1}Se$	
$E_0=2.805$ eV	$\Gamma_c=28$ meV
$\Gamma_i=7$ meV	

[a]Reference 46.
[b]From the measured Raman spectra.
[c]Reference 30.
[d]$\bar{a}=a_H R_H[\epsilon(0)\,E_{Ry}]^{-1}$ (see text).
[e]$Q=(n_L\omega_L+n_S\omega_S)/c$.
[f]Reference 44.
[g]$P\approx 2\pi\hbar/a_0$ (Ref. 45).

the gap energy E_0 and the excitonic broadenings Γ are determined by the spectral position and the broadening of the experimental resonance curves. They were chosen separately for ZnSe, $Zn_{0.97}Mn_{0.03}Se$, and $Zn_{0.9}Mn_{0.1}Se$ in order to obtain the best qualitative agreement between the calculated and the experimental RSE near resonance. The value $E_0=2.800$ eV for ZnSe coincides with the sum of the free exciton energy $E_{ex}=2.782$ eV, determined by photoluminescence excitation spectra,[27] and the exciton Rydberg energy $E_{Ry}=19$ meV. For $Zn_{0.97}Mn_{0.03}Se$ and $Zn_{0.9}Mn_{0.1}Se$ we obtained $E_0=2.798$ and 2.805 eV, respectively. This anomalous dependence of E_0 on the Mn concentration x is in agreement with photoluminescence and reflectivity measurements, reported in Ref. 29. The excitonic broadenings Γ should be expected to increase with increasing x. However, for $Zn_{0.97}Mn_{0.03}Se$ we had to use larger values than for ZnSe and $Zn_{0.9}Mn_{0.1}Se$ (see Table II). This anomaly may be due to the different crystal qualities of the samples. ($Zn_{0.97}Mn_{0.03}Se$ was grown by the Bridgman method while $Zn_{0.9}Mn_{0.1}Se$ was grown from the vapor phase using iodine as a transport agent.) The calculated and the experimental resonance curves differ by scaling factors between 0.25 and 4.5, depending on the scattering geometry and on the Mn concentration x. An inspection of the factors K_{DP} and K_F in Eqs. (8) and (11) shows that these different scaling factors may easily be obtained by slightly varying the parameters P, D_{opt}, C_F, and $\bar{a}$. Note that the values of these x-dependent parameters can be obtained from the literature only within some inaccuracy. Furthermore, it follows from the relations $dS/d\Omega\sim K_{DP}^2$ and $dS/d\Omega\sim K_F^2$ that some of the parameters must be taken to the power of 2, 4, or 6 in order to calculate the RSE. In the case of scattering via deformation potential the effective Bohr radius $\bar{a}$ is related to the RSE by $dS/d\Omega\sim\bar{a}^{-6}$, which means that a small change in the value of $\bar{a}$ would result in a drastic change in the value of $dS/d\Omega$. Nevertheless, we preferred to use the same set of parameters, with the exception of E_0 and Γ, for the calculation of all resonance curves since the variation of one selected parameter seems to be somewhat arbitrary. For the same reason we treated the nonresonant background b_{DP} from Eq. (7) as zero, although a nonzero background could also be used to modify the calculated RSE.

1. *Fröhlich electron-phonon interaction*

One-LO-phonon scattering via intraband Fröhlich electron-phonon interaction can be observed in the scattering configurations $z(x,x)\bar{z}$ and $z''(x,x)\bar{z}''$ (see Table I). In Figs. 3(a)–3(c) the corresponding RSE's for

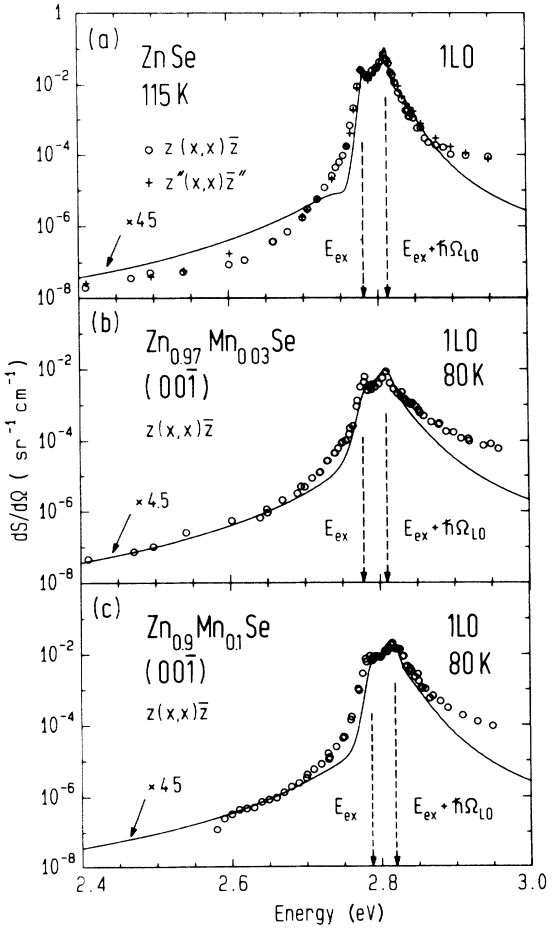

FIG. 3. Experimental RSE for scattering by one LO phonon in (a) ZnSe at 115 K for the scattering configurations $z(x,x)\bar{z}$ and $z''(x,x)\bar{z}''$, (b) $Zn_{0.97}Mn_{0.03}Se$ at 80 K for the scattering configuration $z(x,x)\bar{z}$, and (c) $Zn_{0.9}Mn_{0.1}Se$ at 80 K for the scattering configuration $z(x,x)\bar{z}$. The solid line represents a fit assuming an intrinsic Fröhlich electron-phonon interaction.

ZnSe, $Zn_{0.97}Mn_{0.03}Se$, and $Zn_{0.9}Mn_{0.1}Se$, respectively, are displayed for incident photon energies from 2.4 to 3.0 eV. Both experimental and calculated RSE's exhibit an outgoing resonance at $E_{ex}+\hbar\Omega_{LO}$, which is stronger than the incoming resonance at E_{ex} with $E_{ex}=E_0-E_{Ry}$. The absolute values of the calculated RSE's are smaller than the experimental ones by a factor of 4.5 for all samples using the set of parameters in Table II. However, the relative resonant enhancement of 10^5-10^6 and the qualitative resonance behavior of the experimental RSE are well reproduced by the calculated curves. It should be noted that the value of the calculated RSE at the resonance maximum could easily be adjusted to the experimental value by the choice of smaller excitonic broadenings Γ. But as a consequence the calculated resonance profiles would become sharper than the experimental ones and the qualitative agreement would be lost.

2. *Deformation-potential electron-phonon interaction*

Figures 4(a)–4(c) depict the experimental data, measured in the scattering configuration $z(y,x)\bar{z}$. The experimental data of ZnSe are in excellent agreement with the room-temperature values $dS/d\Omega=7.5\times10^{-7}$ sr^{-1} cm^{-1} for $\hbar\omega_L=2.41$ eV and $dS/d\Omega=3.8\times10^{-6}$ sr^{-1} cm^{-1} for $\hbar\omega_L=2.54$ eV, given in Ref. 30. For this comparison our resonance curve has to be shifted to lower energies by 90 meV in order to take into account the temperature shift of E_0 between 115 and 300 K.[27] According to the selection rules listed in Table I, the observed scattering intensities should be due to deformation-potential interaction. We had to use the scaling factors 1, 0.25, and 0.6 for $Zn_{1-x}Mn_xSe$ ($x=0,0.03,0.1$), respectively, in order to fit the calculated RSE to the experimental data in the low energy range. Experimental and theoretical results differ strongly near resonance. At the resonance maximum the experimental values are one to two orders of magnitude larger than the calculated ones. Furthermore, the experimental RSE exhibits its highest resonance maximum at $E_{ex}+\hbar\Omega_{LO}$ (outgoing resonance), while the calculated RSE reaches it at E_{ex} (incoming resonance). In the case of ZnSe we have also measured the RSE for one TO phonon using the scattering geometry $z''(y'',x)\bar{z}''$. The experimental RSE for LO-phonon scattering is slightly larger than the RSE for TO scattering for incident photon energies below E_{ex}. The difference may be due, in part, to the electro-optic scattering mechanism which has not been included in the calculated Raman polarizability a_{DP} from Ref. 15. For incident photon energies above E_{ex} the TO-phonon Raman intensities decrease very rapidly and could not be discerned from the background above 2.8 eV. In Fig. 4(a) the experimental data for the TO phonon are represented by crosses. Since Raman scattering by TO phonons occurs exclusively via the deformation-potential interaction, the corresponding theoretical resonance curve should be very similar to the one for scattering by LO phonons. Figure 4(a) shows that the experimental resonance behavior of the TO-phonon RSE is in very good agreement with the calculated LO-phonon RSE even above E_{ex}. Therefore, we are led to the assumption that the measured LO-phonon intensities near resonance do not only arise from LO-phonon Raman scattering via deformation-potential interaction, but also from some other scattering mechanism. This assumption is confirmed by the observation of symmetry-forbidden LO-phonon intensities in other scattering configurations.

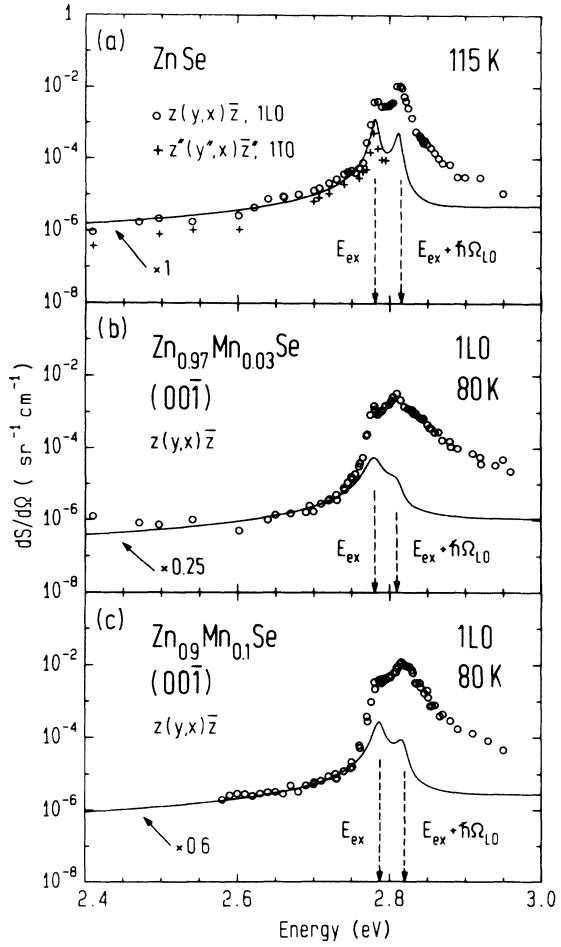

FIG. 4. Experimental RSE for scattering by one LO phonon for the scattering configuration $z(y,x)\bar{z}$ in (a) ZnSe at 115 K, (b) $Zn_{0.97}Mn_{0.03}Se$ at 80 K, and (c) $Zn_{0.9}Mn_{0.1}Se$ at 80 K. The solid line represents a fit assuming an intrinsic deformation-potential electron-phonon interaction. In (a) the experimental RSE for scattering by one TO phonon in the configuration $z''(y'',x)\bar{z}''$ is also shown.

3. *Observation of symmetry-forbidden LO-phonon intensities*

According to the selection rules given in Table I, no LO-phonon Raman signal should be observed in the scattering configurations $z(y',x')\bar{z}$, $z(x',y')\bar{z}$, and $z''(y'',x)\bar{z}''$. However, we observed a strong violation of this Raman selection rule in all investigated samples. Figure 5 shows the corresponding experimental data for ZnSe. The experimental resonance curves for the deformation potential (dotted line) from Fig. 4(a) and Fröhlich interaction (dashed line) from Fig. 3(a) are schematically drawn for comparison. The LO-phonon intensities, measured in symmetry-forbidden configurations, are only observed near resonance. Misalignment or internal stress of

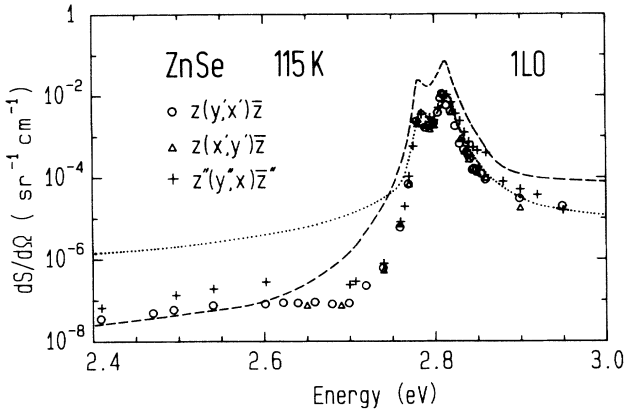

FIG. 5. Experimental RSE for scattering by one LO phonon in ZnSe at 115 K for the scattering configurations $z(y',x')\bar{z}$, $z(x',y')\bar{z}$, and $z''(y'',x)\bar{z}''$. According to Table I no Raman signal should be observed in these scattering configurations. The measured Raman efficiencies in the configurations $z(y,x)\bar{z}$ (· · · ·) and $z(x,x)\bar{z}$ (— — —) are shown schematically for comparison.

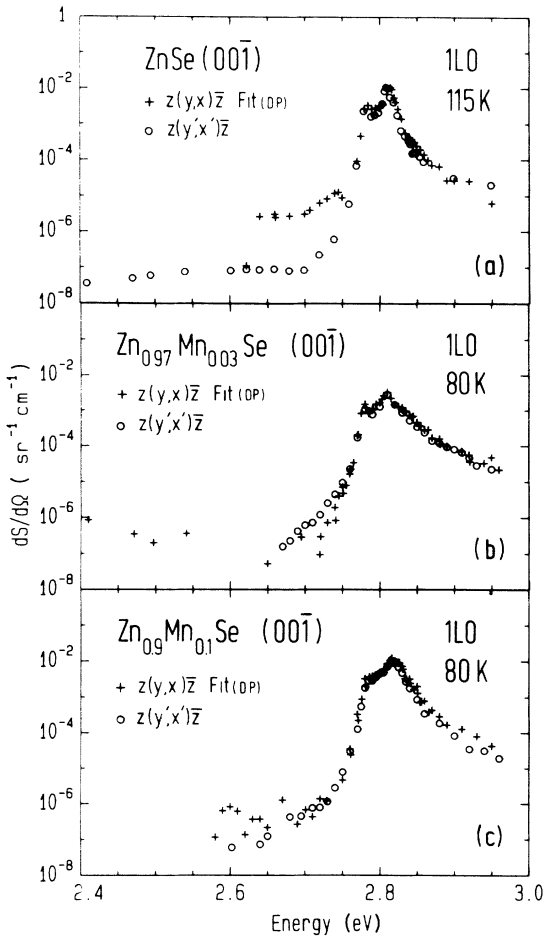

FIG. 6. Symmetry-forbidden LO-phonon intensities (○) in comparison with the difference of experimental data and calculated RSE for $z(y,x)\bar{z}$ (+) in (a) ZnSe, (b) $Zn_{0.97}Mn_{0.03}Se$, and (c) $Zn_{0.9}Mn_{0.1}Se$.

the crystals can be excluded as a possible origin of the observed phenomenon since the Raman selection rules are well fulfilled for incident photon energies below E_{ex}. In $GaAs/Ga_{1-x}Al_xAs$ quantum wells symmetry-forbidden LO-phonon scattering has been explained by a polarization relaxation of excitons produced by the relaxation of the electron and hole spins in the excitonic intermediate states.[31] It is known that elastic scattering by impurities in addition to the inelastic scattering by electron-phonon interaction may lead to a depolarization of the scattered light.[32] Thus, an impurity-induced Fröhlich scattering mechanism[13] connected with a polarization relaxation of the excitons could account for the observed phenomenon. Near resonance the dispersion curves of photons and excitons cross. In the case of strong exciton-photon coupling, exciton polaritons have to be considered as intermediate states, and perturbation theory, which treats excitons and photons as uncoupled excitations, must break down.[33,34] It is a significant feature of polariton-mediated light scattering that the phonon wave vector **Q** must no longer equal the difference of the photon wave vectors $\mathbf{k}_L$ and $\mathbf{k}_S$. Depolarization of the scattered light may be explained by impurity-induced scattering between different polariton branches. If the symmetry-forbidden LO-phonon intensities were actually due to scattering processes where the phase coherence between initial and final intermediate states is lost, they should be observed in all backscattering configurations. Then the discrepancy between theory and experiment for the deformation-potential interaction can qualitatively be explained. In Figs. 6(a)–6(c) it is demonstrated that near resonance the differences between the experimental data and the calculated RSE in Figs. 4(a)–4(c) coincide exactly with the observed symmetry-forbidden LO-phonon intensities for all samples under investigation. For photon energies below E_{ex} the difference curves, represented by crosses, should not be taken too seriously since the subtraction of a smooth calculated curve from experimental data will always give strongly varying results on a logarithmic scale. Recently symmetry-forbidden LO-phonon intensities have been observed also in ZnTe bulk single crystals and MOCVD-grown single-crystal layers.[35] In the case of Fröhlich interaction the superposition of the Raman intensities by symmetry-forbidden LO-phonon intensities does not change the resonance behavior of the RSE significantly. From Fig. 5 it follows that the experimental RSE for scattering by Fröhlich interaction is about one order of magnitude larger than the LO-phonon intensities measured in the forbidden scattering configuration. We have subtracted the forbidden LO-phonon intensities from the experimental data in Figs. 3(a)–3(c) and found that the calculated RSE's are still very good fits to the experimental Fröhlich RSE.

4. Interference of the deformation potential and Fröhlich interaction

The interference of the deformation potential and Fröhlich scattering near critical points is a well-documented phenomenon.[3,4,8,11,36] Clearly different resonance spectra for the configurations $z(x',x')\bar{z}$ and

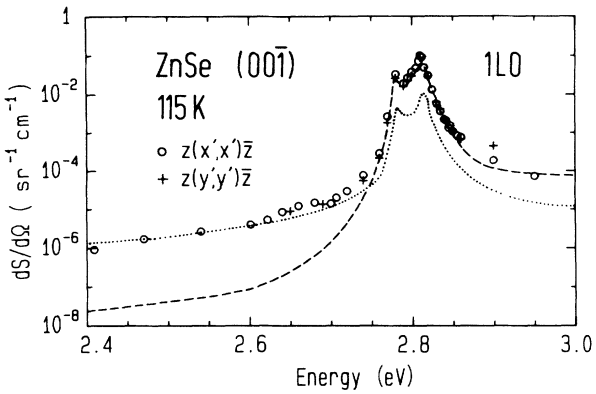

FIG. 7. Experimental RSE for scattering by one LO phonon in ZnSe at 115 K for the scattering configurations $z(x',x')\bar{z}$ and $z(y',y')\bar{z}$. The measured Raman efficiencies in the configurations $z(y,x)\bar{z}$ (· · · ·) and $z(x,x)\bar{z}$ (— — —) are shown schematically for comparison.

$z(y',y')\bar{z}$, corresponding to the Raman polarizabilities $|a_F - a_{DP}|^2$ and $|a_F + a_{DP}|^2$ (see Table I), have been measured in GaP at E_0.[8] In the $Zn_{1-x}Mn_xSe$ samples under investigation no significant differences could be observed between these two configurations within the experimental errors. The measured data for ZnSe are plotted in Fig. 7 and the experimental resonance curves for the $z(x,x)\bar{z}$ scattering configuration from Fig. 3(a) (dashed line) and for the $z(y,x)\bar{z}$ scattering configuration from Fig. 4(a) (dotted line) are schematically drawn for comparison. For incident photon energies below E_{ex} the resonance profile of the RSE is determined by the deformation-potential mechanism and near resonance the Fröhlich mechanism is dominating. Interference between these two scattering mechanisms should be observable only when the corresponding scattering intensities are nearly equal, i.e., at the crossing point of the dashed and dotted line. Possibly an interference structure is present at this point but is too weak to be detected. Thus, Fig. 7 suggests that the resonance spectra for the $z(x',x')\bar{z}$ and $z(y',y')\bar{z}$ configuration are identical and that they can be considered to be just the sum of the resonance curves for $z(y,x)\bar{z}$ and $z(x,x)\bar{z}$.

B. Scattering by two LO phonons

In first-order Raman scattering the LO phonons, involved in the scattering process, are restricted to the center of the Brillouin zone. This is a consequence of wave-vector conservation and the smallness of the wave vectors $\mathbf{k}_L$ and $\mathbf{k}_S$ of the incident and scattered photon, respectively. In second-order Raman scattering wave-vector conservation requires $\mathbf{k}_L - \mathbf{k}_S = \mathbf{Q}_1 + \mathbf{Q}_2 \approx 0$. Thus the two LO-phonon wave vectors $\mathbf{Q}_1$ and $\mathbf{Q}_2$ are only restricted to have nearly equal magnitude and opposite directions. This means that both LO phonons must belong to the same symmetry point, although LO phonons from all over the Brillouin zone may now participate in the scattering process. The most significant LO-phonon

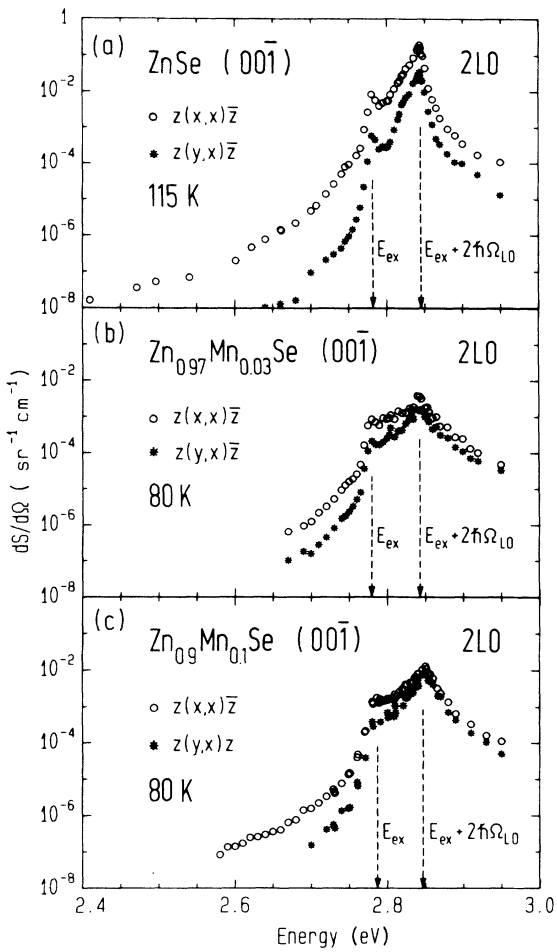

FIG. 8. Experimental RSE for scattering by two LO phonons in the scattering configurations $z(x,x)\bar{z}$ and $z(y,x)\bar{z}$ in (a) ZnSe at 115 K, (b) $Zn_{0.97}Mn_{0.03}Se$ at 80 K, and (c) $Zn_{0.9}Mn_{0.1}Se$ at 80 K.

contribution is expected near the critical ponts Γ, X, L, and W, where singularities in the two-phonon density of states occur. The symmetry properties of the LO-phonon overtones can be derived from the direct product representation of the corresponding one-LO-phonon representations.[37] In Figs. 8(a)–8(c) the experimental RSE for scattering by two LO phonons in $Zn_{1-x}Mn_xSe$ ($x=0,0.03,0.1$) are displayed for the backscattering configurations $z(x,x)\bar{z}$ and $z(y,x)\bar{z}$. In agreement with the different excitonic broadenings Γ, determined from the calculations of the one-LO-phonon resonance curves, the resonance profiles are most pronounced for ZnSe and weakest for $Zn_{0.97}Mn_{0.03}Se$. All resonance spectra exhibit an incoming resonance at E_{ex} and an outgoing resonance at $E_{ex}+2\hbar\Omega_{LO}$. The outgoing resonance is always larger than the incoming one, similar to the case of the one-LO-phonon scattering. In Figs. 9(a) and 9(b) the resonance spectra for ZnSe and $Zn_{0.97}Mn_{0.03}Se$, respectively, are displayed for the scattering configurations $z(x',x')\bar{z}$, $z(y',y')\bar{z}$, $z(y',x')\bar{z}$, and $z(x',y')\bar{z}$. In this section we have not presented a calculated resonance curve for two-LO-phonon scattering, although there exists a large num-

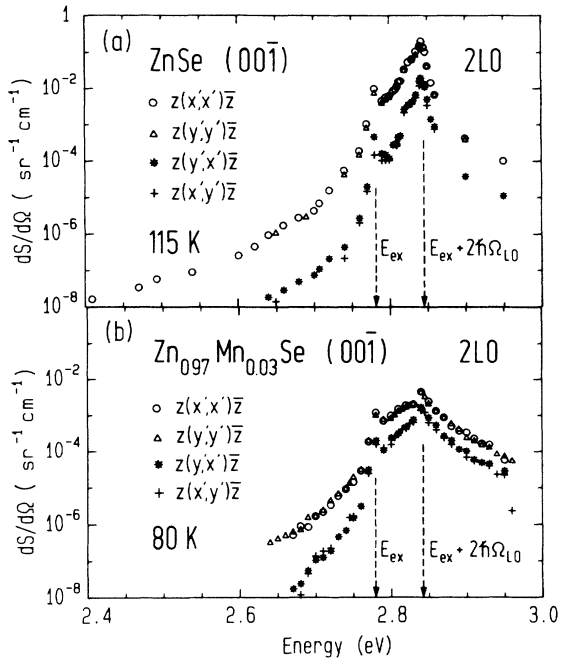

FIG. 9. Experimental RSE for scattering by two LO phonons in the scattering configurations $z(x',x')\bar{z}$, $z(y',y')\bar{z}$, $z(y',x')\bar{z}$, and $z(x',y')\bar{z}$ in (a) ZnSe at 115 K and (b) $Zn_{0.97}Mn_{0.03}Se$ at 80 K.

ber of publications which give suitable analytical expressions.[38–43] The reason is that the theoretical models (or at least the formal parameters used in these models) are not fully consistent with the theoretical exitonic formalism for scattering by one LO phonon, presented in this paper.

V. CONCLUSIONS

We have determined the absolute Raman scattering efficiency for scattering by one and two LO phonons in $Zn_{1-x}Mn_xSe$ ($x=0$, 0.03, and 0.1) near the E_0 gap. All resonance spectra exhibit an outgoing resonance at $E_{ex}+\hbar\Omega_{LO}$ (1 LO) or $E_{ex}+2\hbar\Omega_{LO}$ (2 LO) which is larger than the incoming resonance at E_{ex}. For scattering by one LO phonon we compared our results with calculated Raman scattering efficiencies where the discrete and continuous states of Wannier-Mott excitons have been taken into account. While in the case of Fröhlich electron-phonon interaction experimental and theoretical data show very good agreement, a large discrepancy near resonance has been found for the deformation-potential interaction. In this case the difference of experimental and calculated data coincides exactly with the intensities of symmetry-forbidden LO-phonon lines. The origin of these symmetry-forbidden LO-phonon intensities is not yet exactly known, but we suppose that it is connected with some loss of phase correlation between the intermediate electronic states.

ACKNOWLEDGMENTS

We wish to express our gratitude to M. Cardona for his support at the Max-Planck-Institut, for stimulating discussions, and for a critical reading of the manuscript. We would like to thank W. Giriat, Instituto Venezolano de Investigaciones Cientificas (IVIC), Caracas, and H. H. Otto, Universität Regensburg, for kindly providing us with the $Zn_{0.97}Mn_{0.03}Se$ and $Zn_{0.9}Mn_{0.1}Se$ samples. C. Trallero-Giner thanks the Alexander von Humboldt Foundation for support.

*Permanent address: Drägerwerk AG, Abt. Grundlagenentwicklung, Moislinger Allee 53–55, D-2400 Lübeck, Federal Republic of Germany.

†Permanent address: Departament de Física Aplicada, Universitat de València, Burjassot, E-46100 València, Spain.

‡Permanent address: Department of Theoretical Physics, Havana University, San Lázaro y L, Havana, Cuba.

[1]M. Cardona, in *Light Scattering in Solids II*, Vol. 50 of *Topics in Applied Physics*, edited by M. Cardona and G. Güntherodt (Springer, Berlin, 1982).

[2]W. Richter, in *Solid State Physics*, Vol. 78 of *Springer Tracts in Modern Physics*, edited by G. Höhler (Springer, Berlin, 1976).

[3]J. Menéndez and M. Cardona, Phys. Rev. B **31**, 3696 (1985).

[4]W. Kauschke and M. Cardona, Phys. Rev. B **33**, 5473 (1986).

[5]A. K. Sood, W. Kauschke, J. Menéndez, and M. Cardona, Phys. Rev. B **35**, 2886 (1987).

[6]W. Kauschke and M. Cardona, Phys. Rev. B **35**, 9619 (1987).

[7]W. Kauschke, N. Mestres, and M. Cardona, Phys. Rev. B **36**, 7469 (1987).

[8]W. Kauschke, V. Vorlíček, and M. Cardona, Phys. Rev. B **36**, 9129 (1987).

[9]W. Kauschke, V. Vorlíček, M. Cardona, L. Viña, and W. I. Wang, Solid State Commun. **61**, 487 (1987).

[10]J. Menéndez, M. Cardona, and L. K. Vodopyanov, Phys. Rev. B **31**, 3705 (1985).

[11]W. Kauschke, M. Cardona, and E. Bauser, Phys. Rev. B **35**, 8030 (1987).

[12]W. Kauschke, A. K. Sood, M. Cardona, and K. Ploog, Phys. Rev. B **36**, 1612 (1987).

[13]A. A. Gogolin and E. I. Rashba, Solid State Commun. **19**, 1177 (1976).

[14]W. Limmer, H. Leiderer, and W. Gebhardt, in *Growth and Optical Properties of Wide-Gap II-VI Low-Dimensional Semiconductors*, Vol. 200 of *NATO Advanced Study Institute Series B: Physics*, edited by T. C. McGill, C. M. Sotomayor-Torres, and W. Gebhardt (Plenum, New York, 1989), p. 281.

[15]A. Cantarero, C. Trallero-Giner, and M. Cardona, Phys. Rev. B **39**, 8388 (1989).

[16]C. Trallero-Giner, A. Cantarero, and M. Cardona, Phys. Rev. B **40**, 4030 (1989).

[17]R. Loudon, *The Quantum Theory of Light* (Clarendon, Oxford, 1973).

[18]R. Loudon, Proc. R. Soc. London, Ser. A **275**, 218 (1963).

[19]C. Steineck, W. Limmer, H. H. Otto, and W. Gebhardt, J. Phys. C **21**, 3507 (1988).

[20]A. Alexandrou, C. Trallero-Giner, A. Cantarero, and M. Cardona, Phys. Rev. B **40**, 1603 (1989).

[21]E. O. Kane, in *Semiconductors and Semimetals*, Vol. 1, edited by R. K. Willardson and A. C. Beer (Academic, New York, 1966), p. 75.

[22]J. Wagner and M. Cardona, Solidi State Commun. **48**, 301 (1983).
[23]V. P. Gribkovskii, L. G. Zimin, S. V. Gaponenko, I. E. Malinovskii, P. I. Kuznetsov, and G. G. Yakushcheva, Phys. Status Solidi B **150**, 761 (1988).
[24]D. E. Aspnes and A. A. Studna, Phys. Rev. B **27**, 985 (1983).
[25]W. C. Dash and R. Newman, Phys. Rev. **99**, 1151 (1955).
[26]P. J. Dean and J. L. Merz, Phys. Rev. **178**, 1310 (1969).
[27]Y. Shirakawa and H. Kukimoto, J. Appl. Phys. **51**(4), 2014 (1980).
[28]P. J. Dean, D. C. Herbert, C. J. Werkhoven, B. J. Fitzpatrick, and R. N. Bhargava, Phys. Rev. B **23**, 4888 (1981).
[29]R. B. Bylsma, W. M. Becker, J. Kossut, U. Debska, and D. Yoder-Short, Phys. Rev. B **33**, 8207 (1986).
[30]J. M. Calleja, H. Vogt, and M. Cardona, Philos. Mag. A **45**, 239 (1982).
[31]D. A. Kleinman, R. C. Müller, and A. C. Gossard, Phys. Rev. B **35**, 664 (1987).
[32]G. E. Pikus and E. L. Ivchenko, in *Excitons,* Vol. 2 of *Modern Problems in Condensed Matter Sciences,* edited by E. I. Rashba and M. D. Sturge (North-Holland, Amsterdam, 1982), p. 205.
[33]B. Bendow, in *Polariton Theory of Resonance Raman Scattering in Solids,* Vol. 82 of *Springer Tracts in Modern Physics,* edited by G. Höhler (Springer, Berlin, 1978), p. 69.
[34]C. Weisbuch and R. G. Ulbrich, in *Light Scattering in Solids III,* Vol. 51 of *Topics in Applied Physics,* edited by M. Cardona and G. Güntherodt (Springer, Berlin, 1982), p. 207.
[35]H. Leiderer, K. Jakob, W. Limmer, and W. Gebhardt, unpublished.
[36]A. Cantarero, C. Trallero-Giner, and M. Cardona, unpublished.
[37]J. L. Birman, Phys. Rev. **131**, 1489 (1963).
[38]R. M. Martin, Phys. Rev. B **10**, 2620 (1974).
[39]A. K. Ganguly and J. L. Birman, Phys. Rev. **162**, 806 (1967).
[40]R. Zeyher, Phys. Rev. B **9**, 4439 (1974).
[41]D. C. Hamilton, Phys. Rev. **188**, 1221 (1969).
[42]F. Bechstedt and D. Haus, Phys. Status Solidi B **88**, 163 (1978).
[43]B. Bendow and J. L. Birman, Phys. Rev. B **4**, 569 (1971).
[44]M. Cardona, N. E. Christensen, and G. Fasol, Phys. Rev. B **38**, 1806 (1988).
[45]M. Cardona, in *Atomic Structure and Properties of Solids,* edited by E. Burstein (Academic, New York, 1972).
[46]*Landolt-Börnstein Tables,* Vol. III/22a, edited by O. Madelung and M. Schulz (Springer, Berlin, 1987).